Fabricating Diminishable Visual Markers for Geometric Registration in Projection Mapping

Hirotaka Asayama, Daisuke Iwai, *Member, IEEE*, and Kosuke Sato, *Member, IEEE*

Abstract—We propose a visual marker embedding method for the pose estimation of a projection surface to correctly map projected images onto the surface. Assuming that the surface is fabricated by a full-color or multi-material three-dimensional (3D) printer, we propose to automatically embed visual markers on the surface with mechanical accuracy. The appearance of the marker is designed such that the marker is detected by infrared cameras even when printed on a non-planar surface while its appearance can be diminished by the projection to be as imperceptible as possible to human observers. The marker placement is optimized using a genetic algorithm to maximize the number of valid viewpoints from which the pose of the object can be estimated correctly using a stereo camera system. We also propose a radiometric compensation technique to quickly diminish the marker appearance. Experimental results confirm that the pose of projection objects are correctly estimated while the appearance of the markers was diminished to an imperceptible level. At the same time, we confirmed the limitations of the current method; only one object can be handled, and pose estimation is not performed at interactive frame rates. Finally, we demonstrate the proposed technique to show that it works successfully for various surface shapes and target textures.

Index Terms—Digital fabrication, spatial augmented reality, projection mapping, diminished reality, marker-based tracking.

1 Introduction

DIGITAL fabrication is an emerging technology that has drastically changed many fields such as industrial design, medicine, and education. For example, in the industrial design field, a three-dimensional (3D) prototype with a complex shape and various materials and colors can be printed using a 3D printer once it has been designed on a computer. 3D printers are also useful in surgery planning where doctors can discuss the surgery using printed versions of the organs to be operated on, or in science class, where students can learn about natural phenomena in 3D. While such 3D printers shorten the prototyping process significantly, it still takes several hours to print even a small (e.g., 10×10 cm) object. In addition, the materials and color spaces of such state-of-the-art 3D printing technologies are limited. In the medical and education fields, a 3D object with a moving texture would be an ideal visualization tool to understand a surgery site or learn 3D phenomena. However, the texture of a 3D printed object is static, i.e., it cannot be changed dynamically.

Spatial augmented reality (SAR), or projection mapping, allows us to immediately alter the surface appearance of a physical 3D object using projected imagery [1]. Recent advancements in SAR technologies have made it possible to control the color and texture of a 3D object's surface, visually change its shape, and modify its apparent material properties (i.e., BRDF) [2], [3], [4]. Therefore, we believe that the disadvantages of digital fabrication described above can be compensated for by SAR. Integrating SAR with digital fabrication can enhance the prototyping process such that the color, texture, shape, and material of a mockup fabricated by a 3D printer can be modified directly by projection without re-fabrication in the industrial design field. We envision a prototyping scheme whereby a product designer can assess their idea in such a way that a mockup is printed using a 3D printer and placed directly in front of a projector in an arbitrary location at an arbitrary pose, and its appearance can be modified freely by projection. This scheme would also dramatically change both the medical and educational fields.

We choose SAR rather than other augmented reality (AR) approaches (i.e., video/optical see-through AR) for the following reasons. First, we assume application scenarios where only the surface appearance of printed objects is modified and stereoscopic renderings are not necessary. In such cases, SAR generally provides a better visual experience than other AR approaches because there is no vergence-accommodation conflict in SAR. Second, SAR provides an environment in which multiple people can view augmented objects without holding/wearing any special equipment such as head mounted displays or smart phones. We believe such an environment is suitable for many design/educational/medical applications where multiple people (e.g., designers, students, and doctors) generally share objects placed in front of them for a relatively long time (i.e., more than 10 min). Therefore, we naturally decided to apply SAR in this research. Note that we assume that the users do not have frequent touch interactions with the printed objects in this research. We assume that users use GUIs to modify the objects appearances with projected images, and move their viewpoints to see the projected results from different angles rather than moving the objects by hand.

Our goal is to enhance the usefulness of digital fabrication using SAR, in particular, to make the surface textures of printed objects modifiable. Thus, digital fabrication is a key component of this research. To achieve this goal, we must solve a general but fundamental issue in SAR, i.e., a projector's geometric registration so that it can automatically and accurately map projected images onto a fabricated object. We must correctly estimate the pose of the object with respect to the projector to obtain the relationship between each of the object's surface points and the corresponding

- *H. Asayama, D. Iwai, and K. Sato are with Graduate School of Engineering Science, Osaka, Japan.*

E-mail: see http://www.sens.sys.es.osaka-u.ac.jp/

Manuscript received April 19, 2005; revised August 26, 2015.

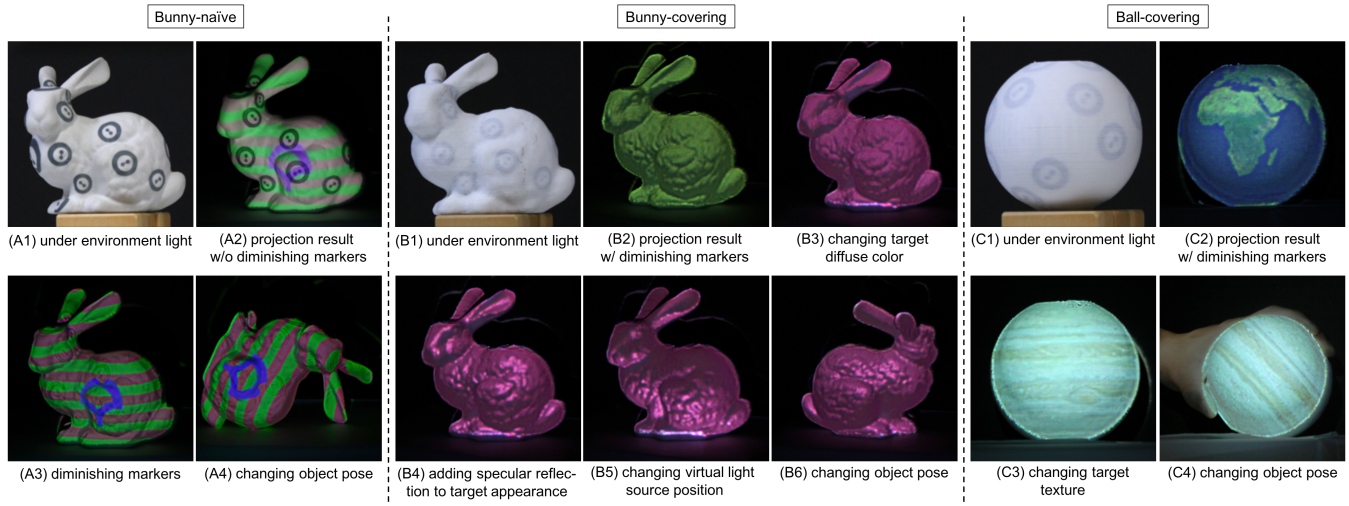

Fig. 1. Projection mapping results on fabricated projection objects with embedded markers: (A) *bunny-naïve*, (B) *bunny-covering*, and (C) *ball-covering* objects. Note that the images were captured using a single-lens reflex (SLR) camera (Canon EOS 550D).

projector pixel illuminating a given point. While various methods have been developed so far, to the best of our knowledge, none are suitable for our target usage scenario. Some previous techniques require user intervention to manually attach markers or sensors to projection objects [5], [6], [7], [8], [9], [10], [11]. Other methods achieve registration by matching between the original model of a mockup and measured information (e.g., camera images or depth maps), which are not applicable to a set of objects whose pose cannot be specified uniquely, such as a sphere, cylinder, or cube [12], [13], [14], [15].

In this paper, we propose a projector geometric registration technique, specifically for an object fabricated by a 3D printer to solve the drawbacks of the techniques described above. The basic idea of the proposed technique is to embed visual markers onto projection objects. When they are fabricated by 3D printers, the markers are printed automatically onto objects of any shape with mechanical accuracy (e.g., 60 μm for a current mid-range fused deposition modeling (FDM) printer). There are two main technical issues that should be considered carefully when designing these fabricated markers. The first issue is marker placement. The 3D position of each marker is measured by a stereo camera system, and the pose of the object is estimated from the 3D layout of the measured positions. Therefore, marker placement should be determined such that the pose of the object is identified uniquely when the cameras capture the object from various viewpoints, where generally only a subset of the markers is observable. We have developed a computational method for marker placement that calculates a placement that satisfies the above requirement and works adaptively according to the object's shape.

The second issue is marker appearance. Embedded markers are generally perceivable under projector illumination, as shown in Fig. 1(A2); therefore, we propose to apply a per-pixel radiometric compensation technique [16] to diminish the visual appearance of the markers. However, even with a state-of-the-art compensation technique [17], it is difficult to diminish marker appearances perfectly in most cases due to the limited dynamic range and spatial resolution of ordinary projectors. For robust marker detection by cameras, the reflectance of the marker should be low while its spatial resolution should be high. In contrast, to diminish the appearance of the marker to an imperceptible level for human observers, the reflectance should be high for better compensation while the spatial resolution should be low, which is less salient for the human visual system. We propose several guidelines for marker appearance design that balance these trade-offs. Finally, we evaluate the proposed method in terms of the accuracy of the pose estimation, position estimation, and imperceptibility performance using a prototype system and objects fabricated using two types of 3D printers. Figure 1 shows examples of the captured images of the fabricated objects and the projection results.

To summarize, this paper provides the following contributions:

- We propose embedding visual markers on a fabricated object's surface using a 3D printer for geometric registration for SAR.
- We introduce marker designing techniques to determine the placement and appearance of markers so that we can estimate the pose of the object robustly while diminishing the appearance of the markers to an imperceptible level.
- We construct a prototype system and evaluate the feasibility of the proposed method using objects fabricated by different types of 3D printers.

2 Related Work

Various techniques for automatic geometric correction of projected images have been proposed to date. For a static projection object, accurate but time-consuming methods have been applied, such as a manual registration approach whereby virtual cross hairs are moved manually to known positions on the object [2] and a structured light pattern projection approach whereby the shape of the object and the projector's intrinsic and extrinsic parameters are estimated from captured patterns [18]. However, we assume that users change the pose of a projection object to assess the projected results from different perspectives. Several techniques that can handle such situations have been proposed. Such techniques generally fall into two categories, i.e., markerless and marker-based techniques.

Markerless methods estimate the six degrees-of-freedom (6DOF) pose of a projection object by matching its original model and measured information, such as color [12], [19], infrared (IR) [13], and depth images [14], [20]. However, it is obvious that such markerless techniques cannot be applied to situations where projection surfaces have either invariant structures (e.g., flat, cylindrical, and spherical surfaces) or periodic shapes (e.g., wavy surfaces) because in such situations the 6DOF pose of the projection surfaces cannot be estimated uniquely. Invariant objects are not rare; they include products for daily use (e.g., cups, dishes, tubes for toothpaste or paint, cylindrical containers for cosmetics such as powder, lamp shades, vases, and bottles), electric devices (e.g., remote controllers and smart phones), and educational tools (e.g., globes and other planet models should be displayed on a sphere object). The unique pose estimation is necessary to correctly augment these objects. Another type of markerless method was proposed by Sueishi et al. [15]. Their method uses a high-speed camera (1,000 fps) to track the movement of a projection object and galvanometer mirrors to quickly direct the projected image onto the object. The tracking is extremely fast and accurate; however, the projection objects are limited to simple shapes (e.g., flat and spherical surfaces), and this approach cannot estimate the pose of the objects, which is required for our target scenario.

Several marker-based approaches have also been proposed. A pioneering work attached a magnetic tracker to a projection object to track its pose [5]. Visual markers have been also applied to estimate the 6DOF pose of a projection object. The applied markers include 2D patterns, such as the ARToolkit marker [6], [7], natural image markers [8], and motion capture retroreflective markers [9], [10]. These marker-based methods solve the limitations of the markerless methods, i.e., they can estimate the 6DOF pose of objects of any shape. However, especially for a 3D projection object, user intervention is required to attach the markers. Furthermore, an additional geometric calibration must be performed to determine where the markers are attached to the object's surface.

The proposed technique is categorized as a marker-based method. We solve the manual marker installation problem by embedding markers directly onto an object using a 3D printer. However, under projection, the markers are visually salient on the object; consequently, the image quality of the projected result is degraded. Therefore, the appearance of the markers must be visually diminished. For video see-through AR, this has been well investigated as diminished reality (DR) [21], [22], [23]. In contrast, significantly fewer studies into DR have been conducted specifically for SAR because of its technological difficulty, i.e., it is difficult to completely diminish a real surface by projection because of the limited dynamic range and spatial resolution of a projector. Inami et al. avoided this problem by applying a retroreflective material as the projection surface [24]. Iwai et al. showed that they could achieve better results in making physical books visually transparent using a radiometric compensation technique [25]. Therefore, we attempt to visually conceal the embedded markers by applying a modified version of a previously proposed radiometric compensation technique [26]. One might think that we should use IR ink, which is invisible to human observers but detectable by an IR camera [27], rather than diminishing the markers by projection. However, to the best of our knowledge, there is currently no commercially available 3D printer that can print textures on the surface of a fabricated object with IR ink. Furthermore, generally, such ink is not completely invisible to a human observer.

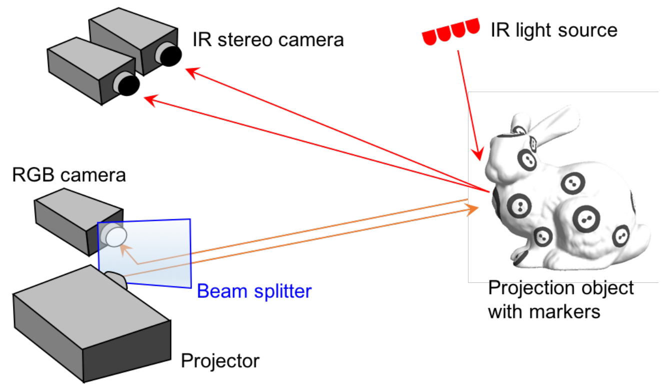

Fig. 2. Overview of the proposed system. The red and orange arrows indicate the IR and visible light rays, respectively.

3 Proposed Method

Here, we describe the proposed method. First, we give an overview of the proposed method, including the system and process flow (Section 3.1). We then explain the core of our proposal, i.e., the fabricated marker design (Section 3.2). Finally, we describe the pose estimation method (Section 3.3) and radiometric compensation technique (Section 3.4).

3.1 Overview

Figure 2 shows an overview of the proposed system, which consists of an IR stereo camera system to estimate the 6DOF pose of a projection object, an RGB camera for radiometric compensation, and a projector. We employ IR cameras to avoid interference from the projected images. The RGB camera and projector are positioned to be optically coaxial using a beam splitter to obtain pixel correspondences independently from the distance to the projection surface.

The proposed method consists of both offline and online processes. In the offline process, we embed visual markers on the 3D model of a projection object and print it using a full-color or multi-material 3D printer. Note that the stereo cameras and RGB camera must be calibrated geometrically to obtain the intrinsic and extrinsic parameters using Zhang's method with a checker board [28]. In addition, pixel correspondences between the RGB camera and the projector also must be obtained. As described above, the correspondences do not vary according to the distance from the lenses because of the coaxial setup. The offline process must be performed once in advance unless any components in the system are changed. In the online process, geometric registration and per-pixel radiometric compensation are performed. First, we estimate the 6DOF pose of a projection object according to the measured 3D positions of the visual markers on the object using the stereo cameras. Radiometric compensation is then performed using the RGB camera to generate a projection image so that the desired colors are displayed while visually diminishing the markers.

3.2 Marker Design

We propose a unique visual marker design for SAR applications assuming that both projection object and markers are fabricated by a 3D printer. In particular, we consider two technical issues, i.e., marker appearance (Section 3.2.1) and marker placement (Section 3.2.2).

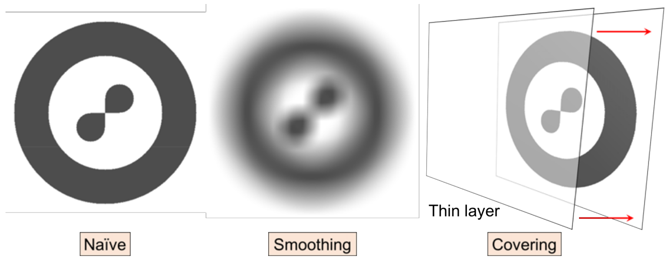

Fig. 3. Proposed marker appearance techniques. The thin layer is opaque (transparent) in the visible (IR) light spectra.

3.2.1 Marker appearance

Generally, embedded markers are perceivable under projector illumination; therefore, we apply a modified version of a per-pixel radiometric compensation technique [26] to visually diminish the markers (Section 3.4). However, it is difficult to diminish marker appearance perfectly in most cases due to the limited dynamic range and spatial resolution of standard projectors. We propose a guideline for designing a marker appearance so that it is robustly and accurately detectable by the stereo cameras while being diminishable by radiometric compensation.

To estimate the 6DOF pose of a projection object, we use the 3D positions of the markers' centers (Section 3.2.2). Therefore, we design the shape of a marker so that its center can be detected even when it is printed on a non-planar surface (Fig. 3). We apply a checker corner for the center of the marker, which can be detected at sub-pixel accuracy regardless of the shape of the printed surface. We also apply a ring shaped frame to increase robustness against image noise; we regard a corner as the center of a marker only when it is inside the frame. This topological relationship is not easily changed, even when the marker is deformed. Note that no identity information is embedded into the proposed marker, whereas such information is typically embedded into other AR markers. This decision was made to avoid a complex marker appearance. Markers with a complex appearance are not detected robustly in the captured images because the markers are typically deformed or even partially occluded on non-planar surfaces. After detecting the marker center with the stereo cameras, we measure the 3D position of the marker using a normal stereo measurement technique.

We determine the reflectance of the marker by balancing the tradeoff between detectability for the stereo cameras and diminishability using radiometric compensation. On one hand, the contrast between the marker and the background (a white projection surface) should be as high as possible in the near IR spectral band so that the stereo cameras can detect the marker successfully. On the other hand, contrast should be as low as possible to obtain better diminishing performance in the visible spectrum by radiometric compensation. We empirically determine the reflectance as follows. We fabricate a flat surface onto which small blobs with different reflectance are embedded. We then check each blob to determine if it can be detected by the IR cameras and can be visually diminished by projection. We then determine the highest reflectance value that satisfies both of the above requirements as the marker reflectance. We refer to this marker appearance technique as the **naïve** methodx (Fig. 3(a)).

To further improve in radiometric compensation performance, we propose the following additional ideas depending on the employed printing technologies. Note that we apply 3D printers that can print an object with different reflectance values. For printers that can output nearly full-color representations, such as inkjet-based full-color (e.g., ProJet CJP 660Pro) and multi-material (e.g., Objet260 Connex3) printers, we apply a low-pass filter (Gaussian filter) to a marker image to blur the edges of the marker (Fig. 3(b)). The window size of the filter is determined to be as large as possible, while the center of the marker can be detected by the IR cameras from the expected measurement distance. We refer to this type of marker appearance technique as **smoothing**. Note that an actual projected pixel is not an infinitesimal dot. Therefore, when a pixel is projected onto an edge, it generally illuminates both the marker and the surrounding background areas. Consequently, the edge of the marker is still visible even if radiometric compensation is applied. The edge is perceptually conspicuous because of the Mach bands effect [29]; thus, we believe that smoothing the marker edges significantly improves the perceived image quality of the marker visual diminishment.

For printers that can output an object with multiple reflectance values but not gradational representation, such as dual extrusion FDM printers (e.g., AW3D HD2X), we cannot apply the low-pass filtering method. Instead, leveraging the difference of the transmittance properties between visible and near IR lights, we propose to cover a projection object uniformly with a thin layer of the material of the background (Fig. 3(c)). We refer to this marker appearance technique as **covering**. The transmittance of IR light is generally higher than that of visible light; thus, the markers are still visible to the IR cameras. However, visible light scatters significantly in this thin layer, which makes the contrast of the marker to the background much smaller and smooths the edge of the marker. Consequently, we believe that this method improves the perceived image quality of the marker visual diminishment significantly.

3.2.2 Marker placement

The 3D position of the central corner of each marker is measured by a stereo camera system, and the 6DOF pose of a projection object is estimated from the 3D layout of the measured positions. Therefore, the marker placement should be determined such that the pose of the object is uniquely identifiable from various viewpoints where generally only a subset of markers is observable by the stereo cameras. We propose a marker placement method whereby placement is computed to satisfy the above requirement depending on the shape of the object. Note that we consider the placement to include both the locations and sizes of the embedded markers.

The proposed method optimizes the number, locations, and sizes of the markers, assuming that the number of markers M is predefined by the user. We use a genetic algorithm (GA) to search for the optimal solution that maximizes the number of valid viewpoints, which is computed as follows. First, we generate a 3D computer graphics model of the projection surface onto which the markers are mapped as a texture. We then render two sets of images of this model using virtual stereo cameras whose centroid is set at a given viewpoint. Then, we consider this viewpoint as valid if the 6DOF pose of the model is estimated accurately from the generated images using a technique described in Section 3.3. We repeat this process for various predefined viewpoints and count the number of valid viewpoints.

We apply the minimal generation gap model [30] for our GA implementation because it gives a globally optimum solution. Suppose that the location v_m and size s_m of each marker

m $(= 1, 2, \ldots, M)$ on the projection surface represents a gene, where an individual solution comprises these genes, i.e., $S = (s_1, \ldots, s_M, v_1, \ldots, v_M)$. During initialization, we generate a population that comprises N_{seed} individual solutions by randomly selecting the sizes and locations of the markers. Then, the following process is repeated N_{loop} times. Two parent solutions are selected randomly from the existing population. Crossover and mutation are applied to the selected parents N_{family} times to generate $2N_{family}$ child solutions. In the mutation process, the number of genes is randomly increased or decreased within a predefined range. We choose two solutions that provide the highest and next-highest numbers of valid viewpoints from the parent and child solutions (i.e., $2+2N_{family}$ solutions). A new population is created with the chosen solutions by replacing the parent solutions. After N_{loop} repetitions, we select the best solution as the optimal marker placement.

A prior work [31] also considers optimal marker layout design for an optical motion tracking system, in which retroreflective markers are attached on rigid body targets. It chooses the marker positions such that the pair-wise marker distances across all targets are not identical. In contrast, as described in this section, our proposed algorithm considers not only the uniqueness of the inter-marker distance but also the marker visibility. In the biomedical research field, optical marker placement is also regarded as an important technological issue. In particular, hadrontherapy requires the occurrence of geometrical deviations of the real target (cancer) to be minimized with respect to the treatment plan in each treatment session. The target position is estimated from an optical motion tracking system, and thus, the deviation depends on the marker placement. Altomare et al. showed that the integration of simulated annealing and pattern search algorithms could provide better marker placement than a normal GA for this purpose [32]. Investigation of more sophisticated algorithms for our system would be one direction for future work.

3.3 Estimation of the 6DOF Pose of a Projection Object

We estimate the 6DOF pose of a projection object as follows. First, we detect the marker center positions in the images captured by the IR stereo cameras. To accomplish this, we binarize the images, by which darker regions, such as the circular frame of a marker, become black. Generally, infrared light sources do not illuminate the projection surface uniformly; thus, simple binarization with a single threshold value does not work properly for the raw captured images. Therefore, we apply a black top-hat transform, which is a morphological image processing technique, to equalize the background prior to the binarization process [33]. We then find closed contours in the binarized image. Finally, we detect the center of the marker by finding the strongest corner surrounded by two of the closed contours. After we obtain the marker center positions in the captured images, we measure their 3D positions by stereo measurement.

The 6DOF pose of the projection object is estimated from the correspondences between the 3D positions of the markers measured by the stereo cameras and those of the original model. However, the appearances of the markers are the same over the surface, as described in Section 3.2.1; therefore, we cannot determine the correspondences directly from the captured images. Instead, we estimate the correspondences by matching the inter-marker distances between the measurement and the model using an approach similar to [31].

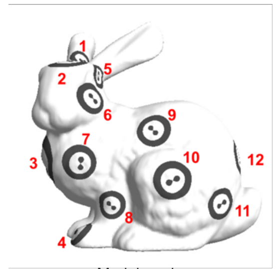

Model markers

$d^{mo}_{i,j}$: distances between markers [mm]

	1	2	3	4	5	6	7	8	9	10	11	12	⋯	M
1		49	22	12	26	20	47	3	3	23	8	26	⋯	24
2	49		3	39	8	33	8	35	4	26	14	21	⋯	7
3	22	3		14	29	15	33	13	28	23	4	11	⋯	6
4	12	39	14		31	34	6	28	13	45	18	47	⋯	31
5	26	8	29	31		21	23	48	33	10	44	37	⋯	35
6	20	33	15	34	21		45	12	36	33	47	47	⋯	41
7	47	8	33	6	23	45		32	37	27	35	19	⋯	6
8	3	35	13	28	48	12	32		6	43	2	15	⋯	42
9	3	4	28	13	33	36	37	6		44	23	18	⋯	2
10	23	26	23	45	10	33	27	43	44		25	31	⋯	6
11	8	14	4	18	44	47	35	2	23	25		44	⋯	11
12	26	21	11	47	37	47	19	15	18	31	44		⋯	43
⋯	⋯	⋯	⋯	⋯	⋯	⋯	⋯	⋯	⋯	⋯	⋯	⋯		34
M	24	7	6	31	35	41	6	42	2	6	11	43	34	

Matching

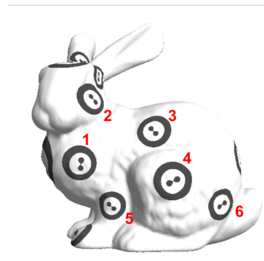

Measured markers

$d^{me}_{i,j}$: distances between markers [mm]

	1	2	3	4	5	6
1		45	37	27	32	35
2	45		36	33	12	47
3	37	36		44	6	23
4	27	33	44		43	25
5	32	12	6	43		2
6	35	47	23	25	2	

Fig. 4. Matching between the model and measured markers. The numbers in the tables are not true values because this figure depicts only the matching process concept.

In the offline process, we compute the distances between all combinations of markers using the 3D model and store them in a database (Fig. 4(top)). We denote the distance between model markers i and j as $d^{mo}_{i,j}$ $(i, j = 1, \ldots, M,\ i \neq j)$. In the online process, we first compute the distances of all combinations of measured markers, which typically comprise only a subset of the model's markers. We denote the distance between two measured markers as $d^{me}_{i,j}$ $(i, j = 1, \ldots, M_{me},\ i \neq j,\ M_{me} \leq M)$, where M_{me} is the number of measured markers (Fig. 4(bottom)). We then search for the correspondences such that all distances between the measured markers are equivalent (or less than a threshold) to those between the corresponding model's markers. The threshold here is set to be slightly smaller than the minimum value of $d^{mo}_{i,j}$. This process is explained as follows. For each measured marker s, we search for candidates of the corresponding model markers in the database. Initially, all the model markers are included in the candidate list of each measured marker s. We exclude model marker u from the candidate list if at least one of the measured distances from s (denoted as $d^{me}_{s,t}$) is not equivalent to all the model distances from u (denoted as $d^{mo}_{u,v}$), i.e., $d^{me}_{s,\exists t} \neq d^{mo}_{u,\forall v}$. Once this process is complete for all measured markers, we search for the correspondences from the candidates in a brute-force manner.

After the correspondences are determined, we estimate the 3D rigid body transformation of the projection object using the singular value decomposition based method [34], [35].

3.4 Radiometric Compensation

Here, we describe our radiometric compensation method to visually diminish markers that are generally perceivable under projector illumination without compensation. In principle, we must capture the reflected intensity of the projected light to determine compensation parameters. For a static scene, parameter calibration is performed in advance, where color patterns are projected and reflectance values are captured. We assume that the pose of a projection object is changed interactively by a user; therefore, we apply a closed-loop approach based on a previously proposed method [26] that computes the radiometric compensation parameters in an online manner.

Generally, radiometric compensation algorithms compute projection color $P_K(x,y)$, $(K=R,G,B)$ to display target color $C_K(x,y)$ at each pixel (x,y). Note that, without loss of generality, we omit (x,y) in the following equations because the compensation works independently of each pixel by assuming a Lambertian surface. Considering the color mixing between the RGB camera and projector, the relationship of P_K and C_K can be expressed as shown below:

$$\mathbf{C}=\mathbf{A}\left(\mathbf{V}\mathbf{P}+\mathbf{E}\right), \tag{1}$$

where $\mathbf{A}$, $\mathbf{V}$, and $\mathbf{E}$ represent the surface reflectance, the color mixing between the RGB camera and the projector, and the intensity of the environmental light, respectively, which are defined as follows:

$$\mathbf{C}=\begin{bmatrix} C_R \\ C_G \\ C_B \end{bmatrix}, \mathbf{A}=\begin{bmatrix} A_R & 0 & 0 \\ 0 & A_G & 0 \\ 0 & 0 & A_B \end{bmatrix}, \mathbf{E}=\begin{bmatrix} E_R \\ E_G \\ E_B \end{bmatrix},$$
$$\mathbf{V}=\begin{bmatrix} V_{RR} & V_{RG} & V_{RB} \\ V_{GR} & V_{GG} & V_{GB} \\ V_{BR} & V_{BG} & V_{BB} \end{bmatrix}, \mathbf{P}=\begin{bmatrix} P_R \\ P_G \\ P_B \end{bmatrix}.$$

When a target color $\mathbf{C}$ is provided, we can compute a color to be projected $\mathbf{P}$ by the following inverse equation:

$$\mathbf{P}=\mathbf{V}^{-1}\left(\mathbf{A}^{-1}\mathbf{C}-\mathbf{E}\right). \tag{2}$$

The previous work [26] proposed a closed-loop algorithm from this model as follows:

$$\mathbf{P}=\mathbf{V}^{-1}\left(\left(\mathbf{A}^{(t-1)}\right)^{-1}\mathbf{C}-\mathbf{E}^{(t-1)}\right), \tag{3}$$

$$A_K^{(t)}=\frac{C_K^{(t)}}{C_K}A_K^{(t-1)}, \tag{4}$$

where t represents the time or frame. The color mixing matrix $\mathbf{V}$ is time invariant and calibrated once in the offline process by projecting five uniformly colored images (i.e., white, black, red, green, and blue) onto a white surface and capturing them using the RGB camera. Here the distance between the projector lens and the white surface is denoted d.

In addition to the previous closed-loop algorithm, we consider the distance between a surface and the projector lens to reduce error in the first iteration. The intensity of projected illumination is physically reduced inversely proportional to the square of the distance. Therefore, we reformulate Eq. (3) as follows:

$$\mathbf{P}=\left(\frac{d^{(t)}}{d}\right)^2\mathbf{V}^{-1}\left(\left(\mathbf{A}^{(t-1)}\right)^{-1}\mathbf{C}-\mathbf{E}^{(t-1)}\right), \tag{5}$$

where $d^{(t)}$ represents the distance at time t, which can be computed from the 3D model and the 6DOF pose of the projector. We implement this radiometric compensation algorithm on a GPU to speed up the process.

4 Experiment

We evaluated the proposed method by investigating how accurately the 6DOF pose of a projection object could be estimated and how well the marker appearamces could be diminished. We compared the results for all proposed marker appearance diminishing methods.

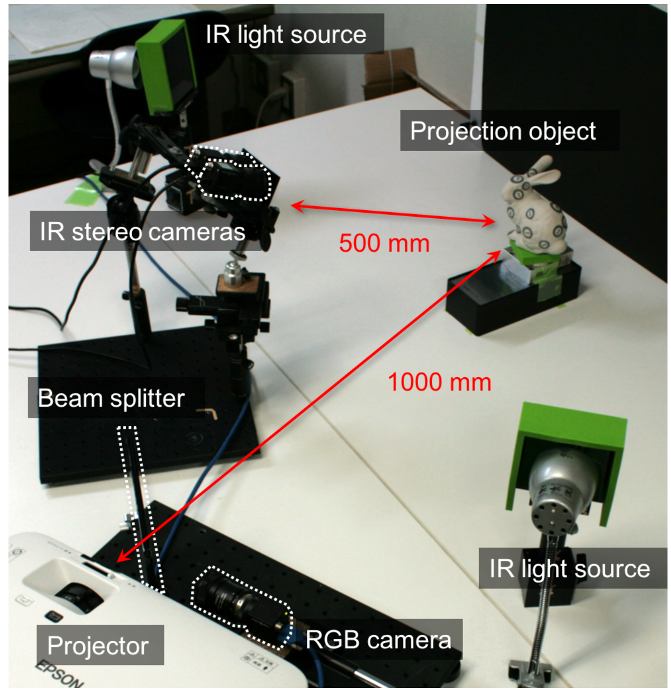

Fig. 5. Experimental setup

4.1 Experimental Setup

We conducted a projection experiment using the prototype system shown in Fig. 5. The experimental setup employed two monochrome cameras (Flea 3 U3-12S2M-CS, 1280×960 pixels) with IR pass filters as the IR stereo cameras, a color camera (Flea 3 U3-13S2C-CS, 1280×960 pixels) as the RGB camera, and a projector (EB1795W, 1280×800 pixels). The RGB camera and the projector shared the same optical axis using a beam splitter. Two IR light sources were placed such that undesirable self-shadows were not cast onto the projection object. This setup ran on an Intel Core i7 (2.4 GHz) platform equipped with 64 GB memory and an NVIDIA Quadro K2200 graphics card.

We fabricated several objects with different shapes and marker appearances. To demonstrate that the proposed method works for a rotationally invariant object, we chose a cone-like shape whose unique pose theoretically cannot be estimated by markerless methods. We fabricated three objects of the same cone shape onto which markers were embedded using different marker appearance techniques (i.e., naïve, smoothing, and covering) for each cone. To demonstrate that the proposed method works for a more complex object, we also fabricated a Stanford Bunny-shaped object with two different marker appearance techniques (i.e., naïve and covering). Specifically, the *cone-naïve*, *cone-smoothing*, and *bunny-naïve* objects were fabricated using an inkjet-based full-color 3D printer (ProJet CJP 660Pro). The RGB colors of (255, 255, 255) and (77, 77, 77) were specified as the background and marker areas of the original textures of these objects, respectively. The *cone-covering* and *bunny-covering* objects were fabricated using a dual extrusion FDM printer (Airwolf 3D HD2X). A white filament (Airwolf Platinum Series ABS Filament, White) was used as the background and thin layer, and a gray filament (Airwolf Platinum Series ABS Filament, Silver) was applied to the embedded markers. The size of the bounding boxes of the objects was 100×100×100 mm for the cone objects and 127×99×126

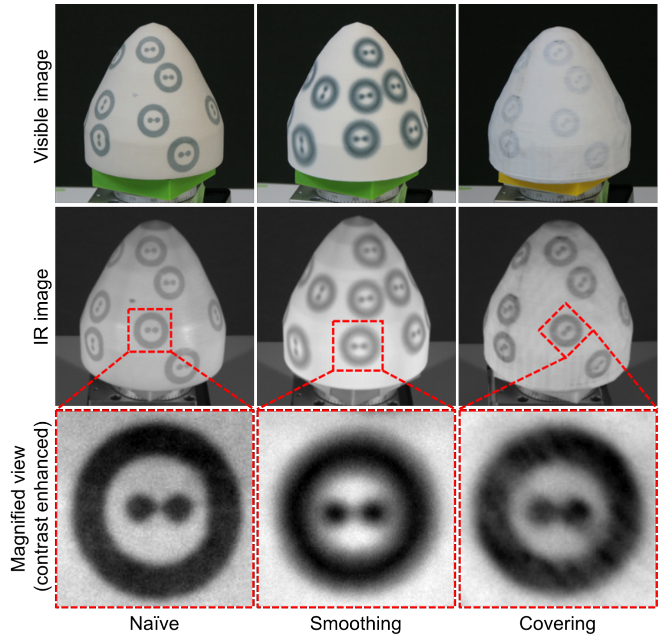

Fig. 6. Marker appearances on cone-shaped objects in RGB and IR images. Note that the visible images were captured using the same SLR camera used for the images in Fig. 1.

mm for the bunny object. The GA parameters for the marker placement were $N_{seed} = 1000$, $N_{family} = 500$, and $N_{loop} = 3000$. The initial number of markers M was 20, and the number of markers in the GA ranged between 15 and 25.

Figure 6 shows the fabricated cone objects captured using both the RGB and IR cameras. We confirmed that the contrast of the embedded markers with the background of the *cone-covering* object was low in the RGB image, and the markers were clearly visible in the IR image. Figure 1(A1) shows the fabricated *bunny-naïve* object. The numbers of markers M were computed to be 17 and 22 for the cones and bunny, respectively.

The pixel correspondences between the projector and the RGB camera were directly obtained using gray code pattern projection. The positions of the detected corner points in the captured IR images were refined at sub-pixel accuracy using the OpenCV function `cornerSubPix` [36].

4.2 Evaluation of Pose Estimation

In the marker placement algorithm (Section 3.2.2), the markers are placed such that the 6DOF pose of the object is estimated correctly from various viewpoints. We conducted two experiments to evaluate this algorithm.

In the first evaluation, we measured reprojection error, which is the 2D Euclidean distance between the measured and estimated marker positions in one of the IR camera image coordinates. The latter was computed from the estimated 6DOF pose of the projection object. Each projection object was placed at 18 different locations with a roughly fixed orientation, and then placed in a roughly fixed location with 13 different orientations. In particular, the location of the object was a center of one of the regular squares (50 mm) composing a 3×3×2 grid that covered the whole measurable volume (Fig. 7(a)). The orientations were selected to include rotations around all three axes. Figure 7(b) shows the captured IR images of *bunny-naïve* for all orientations. The other

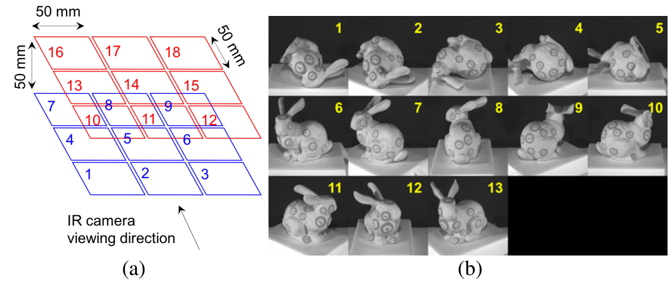

Fig. 7. Locations and orientations of the first evaluation of the pose estimation: (a) 18 locations (the distance between the IR cameras and the center of grid cell 5 was 500 mm) and (b) captured IR images of *bunny-naïve* at 13 orientations.

objects were also placed in the same orientations. The reprojection error was measured 10 times and averaged for each pose. Figure 8 shows the result. The averaged errors of all poses were 0.9 pixels (SD: 0.3) for *cone-naïve*, 0.9 pixels (SD: 0.2) for *cone-smoothing*, 1.3 pixels (SD: 0.3) for *cone-covering*, 1.1 pixels (SD: 0.4) for *bunny-naïve*, and 1.5 pixels (SD: 0.3) for *bunny-covering*.

In the second evaluation, we projected cross-hair patterns whose centers were located at the estimated marker centers computed by the estimated 6DOF pose of a projection object. We then manually measured the distances on the surface between the centers of the projected crosshairs and corresponding printed markers. Figure 9 shows the projected results. As shown in Fig. 10, the averaged distances were 0.9 mm (SD: 0.5) for *cone-naïve*, 1.1 mm (SD: 0.5) for *cone-smoothing*, 1.1 mm (SD: 0.8) for *cone-covering*, 0.8 mm (SD: 0.5) for *bunny-naïve*, and 1.4 mm (SD: 0.7) for *bunny-covering*.

These results indicate that the covering technique was slightly more error prone than the other marker appearance techniques. As shown in the bottom row of Fig. 6, the centers of the captured markers on the *cone-covering* object in the IR images were too unclear to be detected accurately because of the subsurface scattering of IR light. Consequently, the estimation accuracy of the 3D rigid body transformation was degraded for the covering technique. We also found that the errors were nearly the same between the results of the *cone-naïve* and *bunny-naïve* objects. Therefore, it was confirmed that the performance of the proposed marker placement method was not affected by the complexity of the object's shape. In summary, considering the distance from the object to the RGB camera (i.e., approximately 1000 mm), we believe that the errors were sufficiently small to geometrically align projection images with perceptually acceptable accuracies for all marker appearance techniques.

4.3 Evaluation of Marker Visual Diminishment Performance

Marker visual diminishment is a crucial part of this research. The marker visual diminishing performance depends on both the marker appearance and the radiometric compensation methods. Therefore, we compared performance under six different conditions comprising combinations of three marker appearance methods (i.e., the naïve, smoothing, and covering methods) and two radiometric compensation techniques (the previous [26] and proposed techniques). We used the cone-shaped objects as projection objects and a rainbow texture as the target appearance. In this

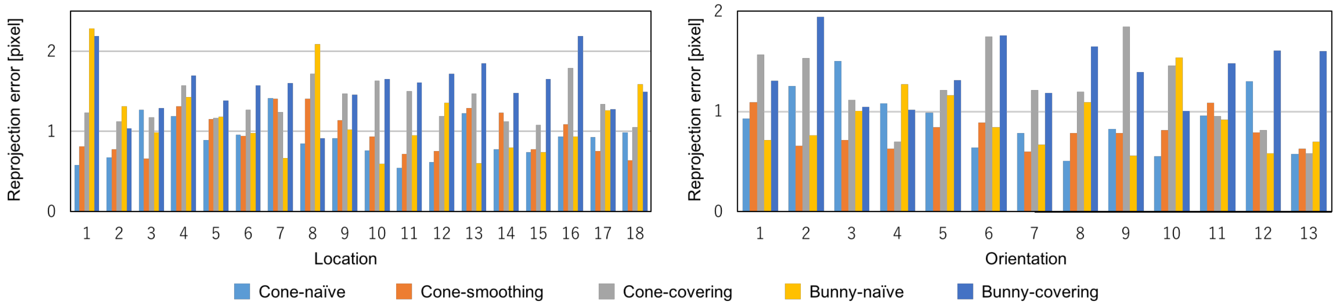

Fig. 8. Reprojection errors.

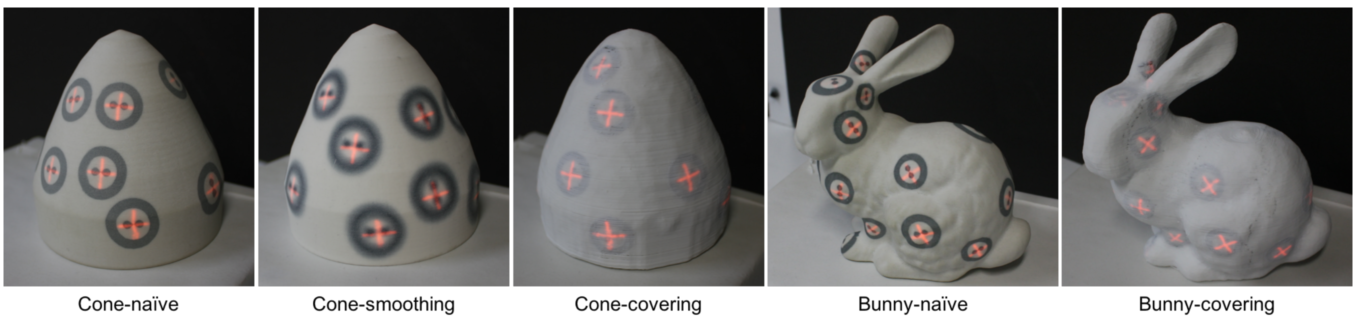

Fig. 9. Projected cross-hair patterns.

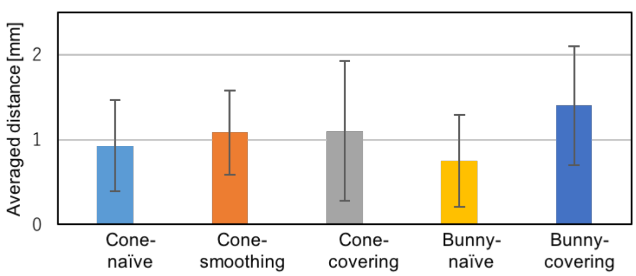

Fig. 10. Averaged distances between the centers of the projected cross-hairs and corresponding printed markers.

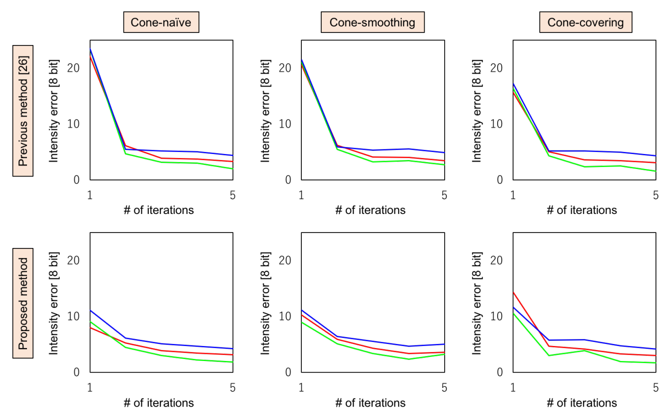

Fig. 11. Averaged intensity errors of RGB channels at each iteration of the previous [26] and proposed radiometric compensation techniques. The red, green, and blue lines represent the errors of the R, G, and B channels, respectively.

evaluation, each of the projection objects was static in front of the projector.

Figure 11 shows the series of RGB intensity errors from the first to fifth iterations of the applied closed-loop radiometric compensation technique for each experimental condition. The errors were computed between a projection result and its target appearance and averaged over the projected surface. Figure 11 includes each combination of marker appearance and radiometric compensation technique. First, we confirmed that the errors were reduced to almost the convergence values in the second iteration under all conditions. Therefore, the marker appearances could be diminished quickly using the radiometric compensation techniques. By comparing the results of the previous [26] and proposed radiometric compensation techniques, we found that the errors in the first iteration were significantly less with the proposed technique. Therefore, even immediately after a projection object is newly placed in front of the system, the proposed technique can alter the appearance of the object by projection with less visual disturbance from the markers than the previous technique.

Figure 12 shows captured images of the projected results at the fifteenth iteration with the proposed radiometric compensation technique. We confirmed that the markers with the covering appearance were visually diminished perfectly, while those with the naïve and smoothing appearances were not. Thus, even after many iterations, the markers were not visually diminished when the naïve and smoothing appearances were applied.

We also conducted a psychophysical experiment, where participants assessed the perceived image qualities of the projected results. Twelve participants (nine males, three females; 22 to 28 years old) were recruited from a local university. We asked them to directly observe each of the projected results shown in Fig. 12 at 1.9 m distance from the objects and rate the image quality based on a 7-point Likert scale (from 1 (markers are not salient) to 7 (mark-

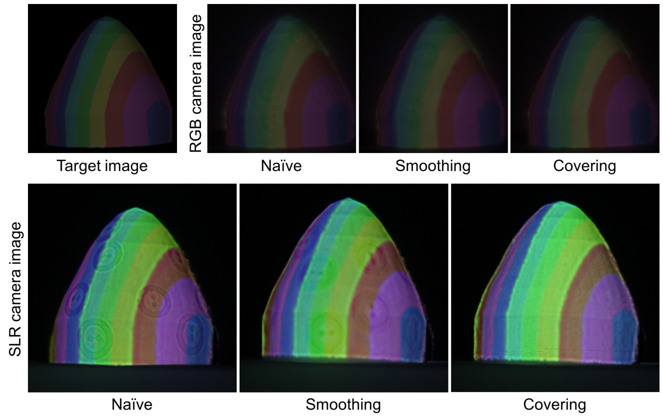

Fig. 12. Marker diminishing results for cone-shaped objects. The top row images represent (left) the target image and (right) the images captured by the system's RGB camera. The bottom row images were captured by the same SLR camera used in Fig. 1 to show that the results are similar to the appearances perceived by human observers.

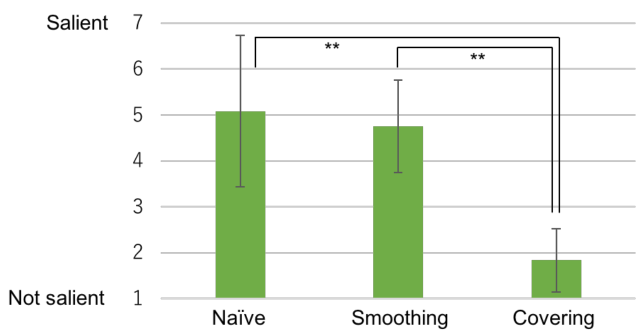

Fig. 13. Results of psychophysical experiment (**: $p < 0.01$).

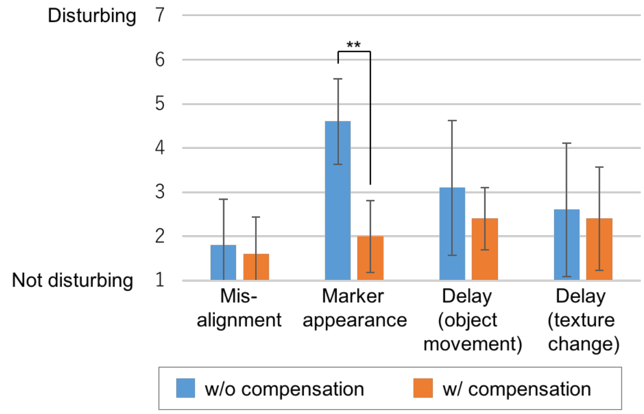

Fig. 14. Usability evaluation results (**: $p < 0.01$).

ers are salient)). Figure 13 shows the results. A one-way repeated measures analysis of variance (ANOVA) revealed a significant difference between the marker appearance techniques ($p < 0.01$). A post-hoc analysis was then performed using Ryan's method for pairwise comparison. The results showed statistically significant differences between the naïve and covering appearances ($p < 0.01$) and the smoothing and covering appearances ($p < 0.01$). These results confirm that the diminishing performance was affected significantly by the marker appearance technique and the covering technique could improve the performance significantly.

4.4 Evaluation of Usability

We conducted another user study to validate the usability of the proposed technique. In the study, participants were asked to design a surface appearance for the *cone-naïve* object. At first, an experimenter handed over the object to each participant. Then, he or she placed it in front of the projector of the proposed system at an arbitrary location within the view volume of the projector with an arbitrary pose. The surface appearance of the object was then modified by the projected imagery. The participant could design the appearance by selecting a texture from five candidates (brick wall, giraffe, cheetah, checker, and spatially uniform patterns) and adjusting the specular reflectance parameter using a graphical user interface displayed on a smartphone. The participant finished the trial when he or she was satisfied the designed appearance. After finishing the trial, the participant responded to a questionnaire consisting of four 7-point Likert scale questions regarding the usability. The questions asked each participant how the following four issues disturbed his or her design process: (1) misalignment of the projected textures, (2) marker appearance, (3) delay due to the object movement, and (4) delay due to the texture change. The participants used a rating of 1 if the issue was not disturbing at all and 7 if it was too disturbing to complete the task.

Because our closed-loop radiometric compensation requires a few frames to converge as shown in Section 4.3, the delay caused by the compensation might be critical for usability. Therefore, we conducted the user study under two different conditions: one with radiometric compensation and the other without compensation.

Twenty participants (seventeen males and three females; 21 to 25 years old) participated from a local university, who were equally divided into two groups. Ten participants performed the trial with the radiometric compensation and the others did it without compensation. The average task completion time was 92.7 and 91.5 s with and without the compensation, respectively. All the participants moved the object and changed the texture and specular reflectance parameter multiple times. The averages and standard deviations of the questionnaire results are shown in Fig. 14. The participants who performed the study with the radiometric compensation rated less than 3 on average for all four issues. Thus, we believe that the usability of the proposed system is acceptable, at least for this particular design process. In contrast, those who performed the study without the compensation rated more than 4 on average for the marker appearance issue. Therefore, we confirmed that the markers should be visually canceled even though the radiometric compensation causes some delays. Note that we performed a paired t-test between the results with compensation and those without compensation of each issue. We confirmed that there was a significant difference only between the results of the marker appearance issue (p <0.01).

5 Discussion

As no identity information is embedded into the markers, the current approach recognizes the markers based on their positions. Regarding this approach, we discuss the following three issues in this paragraph: (1) maker shape, (2) multiple objects handling, and (3) occlusion. (1) One might think that we can replace the current complex markers with simple dots to make the overall process simpler. We tried a random dot marker approach [37] with simple dot markers, but failed to estimate the correct pose of the projection object. This might be mainly because shadows and shades locally change appearances on a non-planar surface, and feature points are not detected at the correct positions. An interesting future work is to try more sophisticated techniques such as those in [38]. (2) The current technique is not designed to work with multiple objects. However, a prior work [31] that takes a similar strategy, i.e., estimates the pose of an object based on marker positions, can handle more than one object by applying a graph search algorithm. Because this approach assumes that all markers are visible to cameras, which is different to our assumption, we cannot directly apply it. It is also an interesting future work to investigate how to modify the current method based on that prior work to handle multiple objects. (3) If the system cannot detect more than four markers because of occlusion, it fails to estimate the pose of a projection object. However, as mentioned in Section 1, we do not assume that users have frequent touch interactions with the printed objects in this research. That is to say, we design our system to support appearance design, rather than interaction design.

The evaluation of the 6DOF estimation (Section 4.2) indicates that the marker appearance of the covering technique is more error prone than the other marker appearances. In contrast, the evaluation of the marker appearance diminishing performance (Section 4.3) shows that the marker appearances of the naïve and smoothing techniques were more perceivable to human observers than the covering technique. Therefore, when applying the proposed technique, we need to consider the advantages and disadvantages of each marker appearance technique. For example, the covering technique would be suitable for many educational and medical scenarios as well as the earlier stages of design scenarios where the geometric alignment of the projected imagery does not need to be perfect. To demonstrate that the covering technique works correctly for shapes other than the cone, we printed two objects (a bunny and a ball), as shown in Figs. 1(B) and 1(C). As shown in the captured images in the figure, we confirmed that the projection images were registered correctly while the marker appearances were diminished to an imperceptible level on these objects. For the later stages of design scenarios, such as in automotive design, the current technique might not be suitable because designers want perfect registration and have a zero-tolerance range for visual artifacts. An interesting future work would be to integrate more accurate projector calibration techniques based on structured light pattern projection [39] and the extended depth-of-field projection technique [40] into the proposed technique to significantly improve the projected results.

The estimation accuracy was not affected by the complexity of the projection object. However, our marker requires a certain area of relatively flat surface to be detected robustly from various viewpoints; thus, the proposed method might not be useful for an object whose surface shape varies more frequently and with more complexity than the bunny-shaped object. Previous markerless geometric correction methods [12], [14] work well for such complex objects; however, they cannot deal with simple objects, as discussed in Section 2. Therefore, future work could be to investigate the effectiveness of a combination of the proposed method and previous markerless techniques for a general object consisting of both simple and complex shapes.

Our current system consists of three components, i.e., a projector, an RGB camera, and IR cameras. Although these components are all necessary to realize geometric correction and radiometric compensation (see [41]), it makes the entire system cumbersome to use and may easily introduce errors due to occlusion. Decreasing the number of system components is also one of our important future tasks.

6 Conclusion

This paper has presented a visual marker embedding method for the pose estimation of a projection surface to correctly map projected images onto the surface. Assuming that the surface is fabricated by a full-color or multi-material 3D printer, we proposed automatically embedding visual markers on the surface at mechanical accuracy. The appearance of the markers was designed so that the marker is detected by infrared cameras even when printed on a non-planar surface while its appearance is diminishable by projections to be as imperceptible as possible for human observes. The marker positions, sizes, and number were computed using a GA to maximize the number of valid viewpoints from which the pose of the object can be estimated correctly using a stereo camera system. We have also proposed a radiometric compensation technique to diminish the marker appearances quickly by extending a previous method. Through our experiments, we have confirmed that the pose of the projection objects could be estimated with accuracy while the markers were diminished to an imperceptible level, and we found that the covering method provided the best marker appearance. We also confirmed that the proposed radiometric compensation technique provided better marker diminishing performance than the previous technique, especially at the first iteration of the closed-loop process. Finally, we demonstrated the proposed technique to show that it works successfully for various surface shapes and target textures.

Acknowledgments

This work has been supported by the JSPS KAKENHI under grant number 15H05925.

References

[1] O.Bimber and R.Raskar, *Spatial Augmented Reality: Mergin Real and Virtual Worlds*. A.K.Peters Ltd., 2005.

[2] R. Raskar, G. Welch, K.-L. Low, and D. Bandyopadhyay, “Shader lamps: Animating real objects with image-based illumination,” in *Proceedings of the 12th Eurographics Workshop on Rendering Techniques*. London, UK, UK: Springer-Verlag, 2001, pp. 89–102.

[3] M. Hisada, K. Takase, K. Yamamoto, I. Kanaya, and K. Sato, “The hyperreal design system,” in *IEEE Virtual Reality Conference (VR 2006)*, March 2006, pp. 313–313.

[4] T. Amano and K. Minami, “Structural Color Display on Retro-reflective Objects,” in *ICAT-EGVE 2015 - International Conference on Artificial Reality and Telexistence and Eurographics Symposium on Virtual Environments*, M. Imura, P. Figueroa, and B. Mohler, Eds. The Eurographics Association, 2015.

[5] D. Bandyopadhyay, R. Raskar, and H. Fuchs, “Dynamic shader lamps : painting on movable objects,” in *Augmented Reality, 2001. Proceedings. IEEE and ACM International Symposium on*, 2001, pp. 207–216.

[6] J. Ehnes, K. Hirota, and M. Hirose, “Projected augmentation - augmented reality using rotatable video projectors,” in *Proceedings of the 3rd IEEE/ACM International Symposium on Mixed and Augmented Reality*, ser. ISMAR ’04. Washington, DC, USA: IEEE Computer Society, 2004, pp. 26–35.

[7] R. Raskar, J. van Baar, P. Beardsley, T. Willwacher, S. Rao, and C. Forlines, “ilamps: Geometrically aware and self-configuring projectors,” *ACM Trans. Graph.*, vol. 22, no. 3, pp. 809–818, Jul. 2003.

[8] D. Molyneaux, H. Gellersen, and J. Finney, “Cooperative augmentation of mobile smart objects with projected displays,” *ACM Trans. Interact. Intell. Syst.*, vol. 3, no. 2, pp. 7:1–7:35, Aug. 2013.

[9] M. R. Marner, R. T. Smith, J. A. Walsh, and B. H. Thomas, "Spatial user interfaces for large-scale projector-based augmented reality," *IEEE Computer Graphics and Applications*, vol. 34, no. 6, pp. 74–82, Nov 2014.

[10] E. Akaoka, T. Ginn, and R. Vertegaal, "Displayobjects: Prototyping functional physical interfaces on 3d styrofoam, paper or cardboard models," in *Proceedings of the Fourth International Conference on Tangible, Embedded, and Embodied Interaction*, ser. TEI '10. New York, NY, USA: ACM, 2010, pp. 49–56.

[11] F. Zheng, R. Schubert, and G. Weich, "A general approach for closed-loop registration in ar," in *2013 IEEE Virtual Reality (VR)*, March 2013, pp. 47–50.

[12] C. Resch, P. Keitler, and G. Klinker, "Sticky projections—a new approach to interactive shader lamp tracking," in *Mixed and Augmented Reality (ISMAR), 2014 IEEE International Symposium on*, Sept 2014, pp. 151–156.

[13] N. Hashimoto and D. Kobayashi, "Dynamic spatial augmented reality with a single ir camera," in *ACM SIGGRAPH 2016 Posters*, ser. SIGGRAPH '16. New York, NY, USA: ACM, 2016, pp. 5:1–5:1.

[14] C. Siegl, M. Colaianni, L. Thies, J. Thies, M. Zollhöfer, S. Izadi, M. Stamminger, and F. Bauer, "Real-time pixel luminance optimization for dynamic multi-projection mapping," *ACM Trans. Graph.*, vol. 34, no. 6, pp. 237:1–237:11, Oct. 2015.

[15] T. Sueishi, H. Oku, and M. Ishikawa, "Robust high-speed tracking against illumination changes for dynamic projection mapping," in *2015 IEEE Virtual Reality (VR)*, March 2015, pp. 97–104.

[16] O. Bimber, D. Iwai, G. Wetzstein, and A. Grundhöfer, "The Visual Computing of Projector-Camera Systems," *Computer Graphics Forum*, 2008.

[17] A. Grundhöfer and D. Iwai, "Robust, error-tolerant photometric projector compensation," *IEEE Transactions on Image Processing*, vol. 24, no. 12, pp. 5086–5099, Dec 2015.

[18] M. R. Mine, J. van Baar, A. Grundhöfer, D. Rose, and B. Yang, "Projection-based augmented reality in disney theme parks," *Computer*, vol. 45, no. 7, pp. 32–40, July 2012.

[19] L. Yang, J. M. Normand, and G. Moreau, "Local geometric consensus: A general purpose point pattern-based tracking algorithm," *IEEE Transactions on Visualization and Computer Graphics*, vol. 21, no. 11, pp. 1299–1308, Nov 2015.

[20] R. F. Salas-Moreno, R. A. Newcombe, H. Strasdat, P. H. J. Kelly, and A. J. Davison, "Slam++: Simultaneous localisation and mapping at the level of objects," in *Computer Vision and Pattern Recognition (CVPR), 2013 IEEE Conference on*, June 2013, pp. 1352–1359.

[21] J. Herling and W. Broll, "Advanced self-contained object removal for realizing real-time diminished reality in unconstrained environments," in *Mixed and Augmented Reality (ISMAR), 2010 9th IEEE International Symposium on*, Oct 2010, pp. 207–212.

[22] N. Kawai, M. Yamasaki, T. Sato, and N. Yokoya, "Diminished reality for ar marker hiding based on image inpainting with reflection of luminance changes," *ITE Transactions on Media Technology and Applications*, vol. 1, no. 4, pp. 343–353, 2013.

[23] J. Herling and W. Broll, "Pixmix: A real-time approach to high-quality diminished reality," in *Mixed and Augmented Reality (ISMAR), 2012 IEEE International Symposium on*, Nov 2012, pp. 141–150.

[24] M. Inami, N. Kawakami, D. Sekiguchi, Y. Yanagida, T. Maeda, and S. Tachi, "Visuo-haptic display using head-mounted projector," in *Virtual Reality, 2000. Proceedings. IEEE*, 2000, pp. 233–240.

[25] D. Iwai and K. Sato, "Document search support by making physical documents transparent in projection-based mixed reality," *Virtual Reality*, vol. 15, no. 2, pp. 147–160, 2011.

[26] K. Fujii, M. D. Grossberg, and S. K. Nayar, "A projector-camera system with real-time photometric adaptation for dynamic environments," in *2005 IEEE Computer Society Conference on Computer Vision and Pattern Recognition (CVPR'05)*, vol. 2, June 2005, pp. 1180 vol. 2–.

[27] P. Punpongsanon, D. Iwai, and K. Sato, "Projection-based visualization of tangential deformation of nonrigid surface by deformation estimation using infrared texture," *Virtual Reality*, vol. 19, no. 1, pp. 45–56, 2015.

[28] Z. Zhang, "A flexible new technique for camera calibration," *IEEE Transactions on Pattern Analysis and Machine Intelligence*, vol. 22, no. 11, pp. 1330–1334, Nov 2000.

[29] D. M. Eagleman, "Visual illusions and neurobiology," *Nature Reviews Neuroscience*, vol. 2, no. 12, pp. 920–926, 2001.

[30] H. Satoh, "Minimal generation gap model for gas considering both exploration and exploitation," *Proc. of the 4th International Conference on Fuzzy Logic, Neural Nets and Soft Computing*, pp. 494–497, 1996.

[31] T. Pintaric and H. Kaufmann, "Affordable infrared-optical pose tracking for virtual and augmented reality," in *IEEE VR Workshop on Trends and Issues in Tracking for Virtual Environments*, G. Zachmann, Ed. Aachen: Shaker Verlag, 2007, pp. 44–51, vortrag: IEEE Virtual Reality 2007, Charlotte, NC (USA); 2007-03-14 – 2007-03-17.

[32] C. Altomare, R. Guglielmann, M. Riboldi, R. Bellazzi, and G. Baroni, "Optimal marker placement in hadrontherapy: Intelligent optimization strategies with augmented lagrangian pattern search," *Journal of Biomedical Informatics*, vol. 53, pp. 65 – 72, 2015.

[33] R. Gonzalez and R. Woods, *Digital Image Processing*. Pearson Education, 2011.

[34] S. Umeyama, "Least-squares estimation of transformation parameters between two point patterns," *IEEE Transactions on Pattern Analysis and Machine Intelligence*, vol. 13, no. 4, pp. 376–380, Apr 1991.

[35] K. Kanatani, "Analysis of 3-d rotation fitting," *IEEE Transactions on Pattern Analysis and Machine Intelligence*, vol. 16, no. 5, pp. 543–549, May 1994.

[36] OpenCV documentation, http://docs.opencv.org/master/, Oct 2016.

[37] H. Uchiyama and H. Saito, "Random dot markers," in *2011 IEEE Virtual Reality Conference*, March 2011, pp. 35–38.

[38] J. Herling and W. Broll, "Random model variation for universal feature tracking," in *Proceedings of the 18th ACM Symposium on Virtual Reality Software and Technology*, ser. VRST '12. New York, NY, USA: ACM, 2012, pp. 169–176.

[39] C. Resch, H. Naik, P. Keitler, S. Benkhardt, and G. Klinker, "On-site semi-automatic calibration and registration of a projector-camera system using arbitrary objects with known geometry," *IEEE Transactions on Visualization and Computer Graphics*, vol. 21, no. 11, pp. 1211–1220, Nov 2015.

[40] D. Iwai, S. Mihara, and K. Sato, "Extended depth-of-field projector by fast focal sweep projection," *IEEE Transactions on Visualization and Computer Graphics*, vol. 21, no. 4, pp. 462–470, April 2015.

[41] O. Bimber, G. Wetzstein, A. Emmerling, and C. Nitschke, "Enabling view-dependent stereoscopic projection in real environments," in *Proceedings of the 4th IEEE/ACM International Symposium on Mixed and Augmented Reality*, ser. ISMAR '05. Washington, DC, USA: IEEE Computer Society, 2005, pp. 14–23.

Hirotaka Asayama received his B.S. degree from Osaka University, Japan, in 2015. He is currently a master course student in Graduate School of Engineering Science, Osaka University, Japan. His research interests include projection mapping and digital fabrication.

Daisuke Iwai received his B.S., M.S., and Ph.D. degrees from Osaka University, Japan, in 2003, 2005, and 2007, respectively. He was a visiting scientist at Bauhaus-University Weimar, Germany, from 2007 to 2008, and a visiting Associate Professor at ETH, Switzerland, in 2011. He is currently an Associate Professor at the Graduate School of Engineering Science, Osaka University. His research interests include spatial augmented reality and projector-camera systems. He is a member of the IEEE.

Kosuke Sato received his B.S., M.S., and Ph.D. degrees from Osaka University, Japan, in 1983, 1985, and 1988, respectively. He was a visiting scientist at the Robotics Institute, Carnegie Mellon University, from 1988 to 1990. He is currently a Professor at the Graduate School of Engineering Science, Osaka University. His research interests include image sensing, 3D image processing, digital archiving, and virtual reality. He is a member of ACM and IEEE.